Acta Crystallographica Section A
Foundations of Crystallography
ISSN 0108-7673

Received 11 July 2000
Accepted 26 September 2000

Forbidden X-ray wavefields of three-beam Bragg reflections from thick crystals

X. R. Huang,* M. Dudley and J. Y. Zhao†

Department of Materials Science and Engineering, State University of New York at Stony Brook, Stony Brook, New York 11794, USA. Correspondence e-mail: xiahuang@ms.cc.sunysb.edu

A detailed analysis of a three-beam diffraction dispersion surface is performed to study the forbidden wavefields of thick-crystal Bragg reflections. From the asymptotic transition between two- and three-beam diffraction, it is found that the excitation state of each wavefield can be accurately determined with the two-beam criterion. Consequently, Bragg-case three-beam diffraction from thick crystals is either a four-mode diffraction process for the Bragg–Laue geometry or a two-mode process for the Bragg–Bragg geometry, and the amplitudes of the excited wavefields can be completely determined by the entrance boundary conditions. Based on this picture, the intrinsic mechanisms underlying three-beam Bragg reflections are clearly illustrated.

1. Introduction

Multiple (N)-beam X-ray diffraction has recently attracted renewed attention due to its applications in solving the phase problem and in analyzing X-ray polarization states (Chapman *et al.*, 1981; Chang, 1984; Shen & Finkelstein, 1992; Hümmer & Weckert, 1996; Weckert & Hümmer, 1997, 1998; Shen, 1998). Although considerable efforts have been made to find approximate but analytical solutions to N-beam diffraction intensity (Juretschke, 1982; Høier & Marthinsen, 1983; Hümmer & Billy, 1986; Shen, 1986, 1999, 2000), the widely used approach is a numerical computation, which is based on the dynamical diffraction theory and can give more accurate results.

Compared to two-beam diffraction, N-beam diffraction involves a much more complicated scattering process but the diffracted intensities from this process can be easily computed using well developed computational algorithms (Colella, 1974; Hümmer & Billy, 1982; Weckert & Hümmer, 1990; Stepanov & Ulyanenkov, 1994), even for cases where a large number of reflections are excited simultaneously. In these algorithms, all the physical aspects related to the scattering process are automatically treated on the basis of the general dynamical theory, which makes it unnecessary to know the calculation details, including the configuration of the dispersion surface (DS), the excitation states of tiepoints, and the treatment of X-ray absorption.

In some cases, however, it may be helpful to analyze the intermediate results, which are usually hidden in the automated computation procedures, so as to obtain a clear understanding of the dynamical diffraction mechanisms. The purpose of this paper is to provide a direct picture of the diffraction process for the commonly used three-beam diffraction. We will focus on the main properties of Bragg-case diffraction from semi-infinite crystals since this geometry exhibits a number of interesting phenomena similar to the well known properties of two-beam diffraction, such as forbidden wavefields, extinction and total reflection. Our calculations presented below will display explicitly the transition between two- and three-beam cases and the similar excitation states of tiepoints on the DS's. We will also discuss the difference between the thick- and thin-crystal diffraction models.

2. Computational procedure

In three-beam diffraction involving two reflections **h** and **g**, the wave equations are

$$[(K^2 - k_i^2)/k_i^2]\mathbf{D}_i + \sum_j \chi_{i-j}\mathbf{D}_{j[i]} = 0 \quad (i, j = 0, h, g), \qquad (1)$$

where K is the magnitude of the incident wavevector (in vacuum), the k_i's are the magnitudes of the internal wavevectors, and the other symbols have well known meanings (Pinsker, 1978). To change (1) into scalar equations, we adopt the coordinate system of Fig. 1, in which the xz plane is the two-beam scattering plane for the primary reflection **h** and the polarization vectors for this reflection are defined according to the two-beam convention. For reflection **g**, $\mathbf{k}_g$ generally does not lie in the xz plane, and the unit vector along $\mathbf{k}_g$ must be

† Present address: Argonne National Laboratory, APS/XFD 431/D003, Argonne, IL 60439, USA.

written as $\mathbf{s}_g = n_1\mathbf{x} + n_2\mathbf{y} + n_3\mathbf{z}$, where $\mathbf{x}$, $\mathbf{y}$, $\mathbf{z}$ are unit vectors along x, y, z axes, respectively. If we let one polarization vector of $\mathbf{D}_g$ be

$$\boldsymbol{\sigma}_g = n_x\mathbf{x} + n_z\mathbf{z},$$

where $n_x = n_3/(n_1^2 + n_3^2)^{1/2}$ and $n_z = -n_1/(n_1^2 + n_3^2)^{1/2}$ (or $n_x = 1$, $n_z = 0$ if $\mathbf{s}_g = \pm\mathbf{y}$), the other polarization vector becomes

$$\boldsymbol{\pi}_g = \mathbf{s}_g \times \boldsymbol{\sigma}_g = n'_x\mathbf{x} + n'_y\mathbf{y} + n'_z\mathbf{z}.$$

Substituting $\mathbf{D}_i = D_{i\sigma}\boldsymbol{\sigma}_i + D_{i\pi}\boldsymbol{\pi}_i$ in (1), one obtains the following wave equations:

$$\begin{pmatrix} \tau_0 & 0 & \chi_{\bar{h}} & 0 & 0 & \chi_{\bar{g}}n'_y \\ 0 & \tau_0 & 0 & \chi_{\bar{h}}\cos 2\theta_B & \chi_{\bar{g}}u_1 & \chi_{\bar{g}}u_3 \\ \chi_h & 0 & \tau_h & 0 & 0 & \chi_{h-g}n'_y \\ 0 & \chi_h\cos 2\theta_B & 0 & \tau_h & \chi_{h-g}u_2 & \chi_{h-g}u_4 \\ 0 & \chi_g u_1 & 0 & \chi_{g-h}u_2 & \tau_g & 0 \\ \chi_g n'_y & \chi_g u_3 & \chi_{g-h}n'_y & \chi_{g-h}u_4 & 0 & \tau_g \end{pmatrix} \begin{pmatrix} D_{0\sigma} \\ D_{0\pi} \\ D_{h\sigma} \\ D_{h\pi} \\ D_{g\sigma} \\ D_{g\pi} \end{pmatrix} = 0, \tag{2}$$

where

$$\tau_i = \chi_0 + (K^2 - k_i^2)/k_i^2$$
$$u_{1(2)} = n_z\cos\theta_B + (-)\, n_x\sin\theta_B$$
$$u_{3(4)} = n'_z\cos\theta_B + (-)\, n'_x\sin\theta_B$$

and θ_B is the Bragg angle of reflection $\mathbf{h}$. The DS is then determined by $|\mathbf{T}| = 0$, where $\mathbf{T}$ is the 6×6 matrix in (2).

The most accurate method for solving the dispersion equation of N-beam diffraction was developed by Colella (1974), which is to calculate the eigenvectors of a $4N \times 4N$ scattering matrix and is applicable for any diffraction conditions. Stepanov & Ulyanenkov (1994) then showed that the matrix rank can be reduced by disregarding the wide-angle specularly reflected beams. In fact, if no grazing beam is involved, the scattering matrix related to $\mathbf{T}$ for the three-beam case has the simplest 6×6 form (Hümmer & Billy, 1982). For simplicity, here we only consider the cases with no beam satisfying the grazing condition or the extreme backward diffraction and we use the non-standard root-searching method to solve $|\mathbf{T}| = 0$ directly.

In Fig. 1, the deviation of the actual incidence wavevector $\mathbf{K}_0$ from $\mathbf{K}_0^0$, the incident wavevector corresponding to the exact three-beam geometrical diffraction position L, is expressed as $K(\omega\mathbf{a}_\theta + \psi\mathbf{a}_\psi)$, where $\mathbf{a}_\psi$ is the direction of the so-called 'azimuthal scan' (ψ scan) while $\mathbf{a}_\theta$ is along the $\mathbf{h}$ rocking-curve scan direction. Owing to the boundary conditions at the entrance surface, each wavevector $\mathbf{k}_j$ inside the crystal is different from the corresponding vacuum wavevector $\mathbf{K}_j$ by a component $K\delta\mathbf{n}_s$ along the surface normal ($j = 0, h, g$). Here

$$\mathbf{K}_0 = \mathbf{K}_0^0 - K(\omega\mathbf{a}_\theta + \psi\mathbf{a}_\psi)$$

and, for $j = h$ and g,

$$\mathbf{K}_j = \mathbf{K}_0^0 + \mathbf{j} - K(\omega\mathbf{a}_\theta + \psi\mathbf{a}_\psi) = \mathbf{K}_j^0 - K(\omega\mathbf{a}_\theta + \psi\mathbf{a}_\psi).$$

Thus, each wavevector inside the crystal is

$$\mathbf{k}_j = \mathbf{K}_j^0 - K(\omega\mathbf{a}_\theta + \psi\mathbf{a}_\psi) - K\delta\mathbf{n}_s, \tag{3}$$

where $j = 0, h, g$. Based on this, the three geometrical diffraction wavevectors satisfy

$$|\mathbf{K}_0^0| = |\mathbf{K}_h^0| = |\mathbf{K}_g^0| = K,$$

and the diagonal elements of $\mathbf{T}$ can be linearized in the vicinity of L as (Pinsker, 1978):

$$\tau_0 \simeq \chi_0 + 2\gamma_0\delta,$$
$$\tau_{h,g} \simeq \chi_0 + 2(\omega\mathbf{a}_\theta + \psi\mathbf{a}_\psi)\cdot\mathbf{s}_{h,g} + 2\gamma_{h,g}\delta, \tag{4}$$

where $\mathbf{s}_j = \mathbf{k}_j/|\mathbf{k}_j|$ and $\gamma_j = \mathbf{n}_s\cdot\mathbf{s}_j$ for $j = 0, h, g$. Then, the dispersion equation can be transformed into a six-degree polynomial equation:

$$f(\delta) = \delta^6 + A_1\delta^5 + \ldots + A_5\delta + A_6 = 0. \tag{5}$$

For the non-absorbing case we will consider in the following, it can be verified that all the coefficients A_j are real numbers. Under this condition, (5) may be conveniently solved by *Bairstow's method* (Press *et al.*, 1988), for both real and complex roots. Subsequently, we can find from any five of the six linear equations in (2) an 'eigenvector' for each root of (5).

For non-absorbing crystals, the dispersion equation (5) of the Laue geometry ($\gamma_h > 0$ and $\gamma_g > 0$) always has six real roots. For Bragg cases ($\gamma_h < 0$ or $\gamma_g < 0$), however, (5) may have conjugate complex roots, and the complex roots correspond to the 'gaps' of the DS where X-ray extinction occurs. Note that if absorption is considered the roots of (5) are usually complex in the entire angular range, and then it becomes difficult to separate extinction from normal absorption. Therefore, it is convenient to neglect absorption for studying the DS structure.

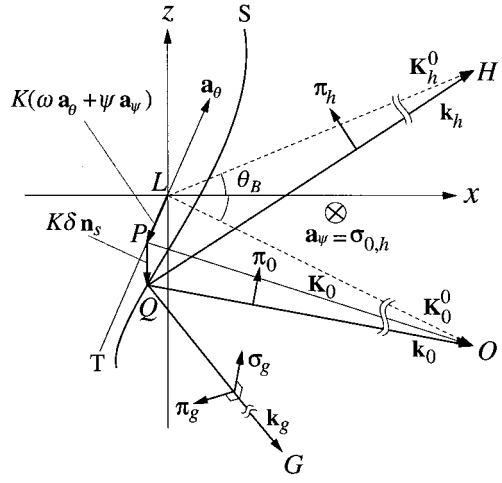

Figure 1
Three-beam diffraction geometry (projection onto the xz plane). L is the three-beam Laue point; T is a sphere (nearly a plane near L) of radius K centered at the reciprocal origin O; $\mathbf{a}_\theta = \sin\theta_B\mathbf{x} + \cos\theta_B\mathbf{z}$ and $\mathbf{a}_\psi = \mathbf{y}$ are two orthogonal unit vectors perpendicular to $\mathbf{K}_0^0$, the incident wavevector corresponding to the exact Bragg condition; S represents the DS; $\mathbf{n}_s$ is the inward normal to the entrance surface.

3. Bragg–Laue case

Let us consider the Bragg–Laue 004|040 reflections of GaAs[1] with 004 being the symmetrical Bragg reflection and 040 undergoing Laue transmission diffraction. We choose the calculation parameters as: incident wavelength $\lambda = 1.54$ Å, involved structure factors $F_{000} = 256$, $F_{004} = F_{040} = 163$ and $F_{044\bar{}} = 129$ (electrons). Fig. 2 shows the root conditions of (5) in the $\omega\psi$ plane (the coordinate axes being $\mathbf{a}_\omega$ and $\mathbf{a}_\psi$). When the incidence direction falls in the gray or black regions, (5) has complex roots. It is apparent that the vertical non-white columns correspond to the full excitation regions of reflection 004 while the inclined stripes are related to 040. The intersection of these stripes thus represents the full excitation region of three-beam diffraction, and the displacement of this region from the Laue point L arises from the small refraction effect.

For three-beam diffraction, the DS consists of six branches (sheets) in the reciprocal space and the map in Fig. 2 actually results from the projection of these sheets onto the $\omega\psi$ plane. To obtain a detailed picture of the three-dimensional DS, we have to examine the sections of these sheets on a set of planes perpendicular to $\mathbf{a}_\psi$.

As a reference, Fig. 3(a) shows the DS of the pure two-beam 004 Bragg reflection based on the analytical solutions

$$\delta = \omega\cos\theta_B \pm [(\omega\sin 2\theta_B + \chi_0)^2 - C^2|\chi_h|^2]^{1/2}/2\sin\theta_B, \quad (6)$$

where C is the two-beam polarization factor. Then the three-beam DS and its evolution with ψ are plotted in Figs. 3(b)–3(f). The DS is actually represented in the $\omega\psi\delta$ coordinate system where the positive direction of the δ axis is along the inward normal $\mathbf{n}_s$ of the entrance surface. Note that the ω axis is along $\mathbf{a}_\theta$ in Fig. 1, but in Fig. 3 we rotated this axis to be horizontal. Thus, the DS is distorted with respect to the actual DS in the reciprocal space. The current representation is convenient for our calculation process and the distortion does not change the physical quantities involved.

In Fig. 3(b), as the azimuthal ψ angle is deviated away from the full excitation region of three-beam diffraction, the main DS (half sheets labeled by S_1, S_2, S_3 and S_4) near the central region is similar to the two-beam DS in Fig. 3(a), indicating that these sheets are closely related to reflection 004. However, two additional sheets (S_5) at the lower region are induced due to reflection 040. These two sheets 'intersect' sheets S_2 at the bottom-left corner, splitting each sheet labeled by S_2 (or S_5) into two parts, S_2 and S_2' (S_5 and S_5'), separated by two 'gaps' G_3 and G_4.

On moving along the positive direction of ψ, the two gaps at the left side move toward the full excitation center, and further move to the upper-right corner when ψ has a large positive value (Fig. 3f). In the full excitation region (Fig. 3d), the four gaps are close to each other, giving rise to strong interactions between the two reflections. Note that all the gaps in Fig. 3 correspond to complex-root regions in Fig. 2. Therefore, the evolution of the gaps with varying ψ can be more clearly understood from Fig. 2.

The six-layer DS corresponds to the fact that there are six possible 'eigenvectors' for each incidence direction (ω, ψ). For a thin plate, the eigenvector strengths can be determined by exactly six boundary-condition equations: four at the entrance surface and two at the back surface. For a semi-infinite crystal, however, the latter two equations do not exist, indicating that only four wave modes are permitted. Therefore, it is important to understand the excitation state of each wave for the semi-infinite-crystal case. This is an easy task when (5) has two pairs of conjugate complex roots (corresponding to the black areas in Fig. 2 or the 'double-gap' angular ranges in Fig. 3). Under this condition, the wave modes corresponding to the roots with negative imaginary parts are naturally forbidden since they would lead to increasing wave amplitudes toward the inside of the crystal. For other situations, however, it becomes complicated and we have to recall the two-beam diffraction principles.

It is well known that tiepoints on the half sheets S_2 and S_3 in Fig. 3(a) are not excited for two-beam Bragg reflection from semi-infinite crystals (forbidden tiepoints). The reason is that these forbidden tiepoints correspond to X-ray energy flows propagating toward the entrance surface. From the mathematical viewpoint, the waves related to the forbidden tiepoints can lead to infinitely increasing amplitudes with increasing angular deviation (ω) of the incidence (Pinsker, 1978; Authier, 1996).

For the three-beam case, one can see that, as the value of ψ increases toward either the negative or the positive direction, the three-beam case asymptotically transforms into a two-beam case. Owing to such an asymptotical behavior, half

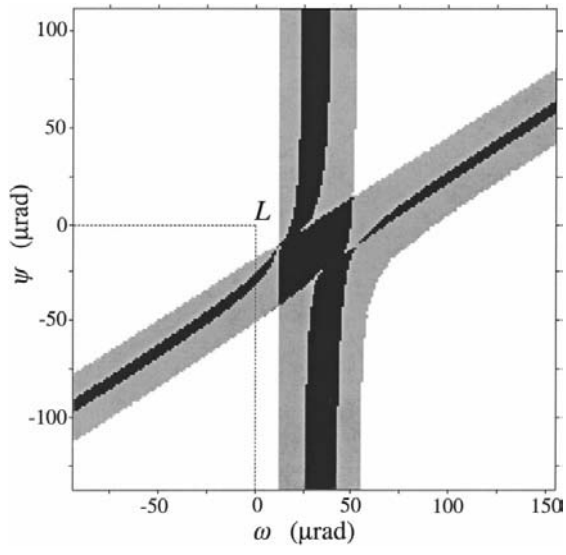

Figure 2
Root conditions of the dispersion equation (5) as a function of ω and ψ. Equation (5) has six real roots in the white regions, four real roots and a pair of conjugate complex roots in the gray regions, and two real roots and two pairs of conjugate complex roots in the black regions.

[1] The GaAs 004|040 (or 004|1$\bar{1}$3 in §4) is a four-beam case in reality since 044 (1$\bar{1}$1 for 004|1$\bar{1}$3) is also excited. Therefore, the calculations presented are based on hypothetical three-beam cases with the third reflection being artificially excluded, but this does not affect our theoretical discussions of three-beam diffraction.

sheets S_2, S_2' and S_3 in Figs. 3(*b*)–3(*f*) have very similar properties as S_2 and S_3 in Fig. 3(*a*). In fact, they form continuous surfaces in the three-dimensional reciprocal space. Thus, it is reasonable to assume that all tiepoints on the same three-dimensional half sheet have the same excitation state. Based on this assumption, tiepoints on all the half sheets S_2, S_2' and S_3 in Figs. 3(*b*)–3(*f*) should be forbidden tiepoints. Such a principle can be verified by the following detailed calculations of the diffracted intensities.

In Figs. 3(*b*)–3(*f*), if the complex roots with negative imaginary parts and the real roots corresponding to the tiepoints on the six DS half sheets labeled by S_2, S_2' and S_3 are disregarded, only four roots of (5) are left in the entire angular region, corresponding to four eigenvectors for each incidence direction (ω, ψ). Then the complex strength q_i of each eigenvector can be easily determined by the four boundary equations at the entrance surface:

$$\begin{aligned} \sum_{i=1}^{4} q_i D_{0\sigma}^{(i)} &= D_{\sigma}^{(a)}, \qquad \sum_{i=1}^{4} q_i D_{0\pi}^{(i)} = D_{\pi}^{(a)}, \\ \sum_{i=1}^{4} q_i D_{g\sigma}^{(i)} &= 0, \qquad \sum_{i=1}^{4} q_i D_{g\pi}^{(i)} = 0, \end{aligned} \tag{7}$$

where $\mathbf{D}^{(a)} = D_{\sigma}^{(a)}\boldsymbol{\sigma}_0 + D_{\pi}^{(a)}\boldsymbol{\pi}_0$ is the amplitude of the incident beam. Finally, the reflected beam is represented by

$$\mathbf{D}_h^{(a)} = \boldsymbol{\sigma}_h \sum_{i=1}^{4} q_i D_{h\sigma}^{(i)} + \boldsymbol{\pi}_h \sum_{i=1}^{4} q_i D_{h\pi}^{(i)}. \tag{8}$$

Fig. 4 shows six calculated 004 ω-scan rocking curves (diffracted intensity represented by the reflectivity R_{004}) corresponding to the DS's in Fig. 3. Here we have used a plane-wave incident beam with $D_{\sigma}^{(a)} = 1$ and $D_{\pi}^{(a)} = 0$. The different rocking curves are mainly the results of the interference between the directly diffracted waves from 004 reflection and the *Umweg* waves arising from the detour reflections 040 and $04\bar{4}$. The correctness of the calculations can be proved by the following facts. First, the main characteristics of the ω-scan rocking curves at large ψ values are very close to that of the two-beam rocking curve (Figs. 4*b* and 4*f*). The only difference is that the small influence of the detour reflections makes the 004 rocking curve slightly asymmetric, but such an asymmetric feature disappears when ψ becomes extremely large. Second, our detailed calculations show that, for each incidence direction (ω, ψ), the reflectivity of reflection 004 is always less than or equal to 1. This is consistent with the energy conservation principle. We have also found that if an excited eigenvector is replaced by a non-excited eigenvector (even if the difference between the two roots is small), the reflectivity can vary irregularly or can be infinitely large.

The most convincing proof is the variation of the integrated intensity I_{004},

$$I_{004}(\psi) \propto \int R_{004}(\psi, \omega)\, \mathrm{d}\omega, \tag{9}$$

with ψ. The thick solid curve in Fig. 5 shows the ψ-dependent integrated intensity profile calculated with the parameters used above (the *invariant triplet phase* Φ being zero). We have also artificially assigned non-zero values to Φ in order to demonstrate the phase effect. The other three

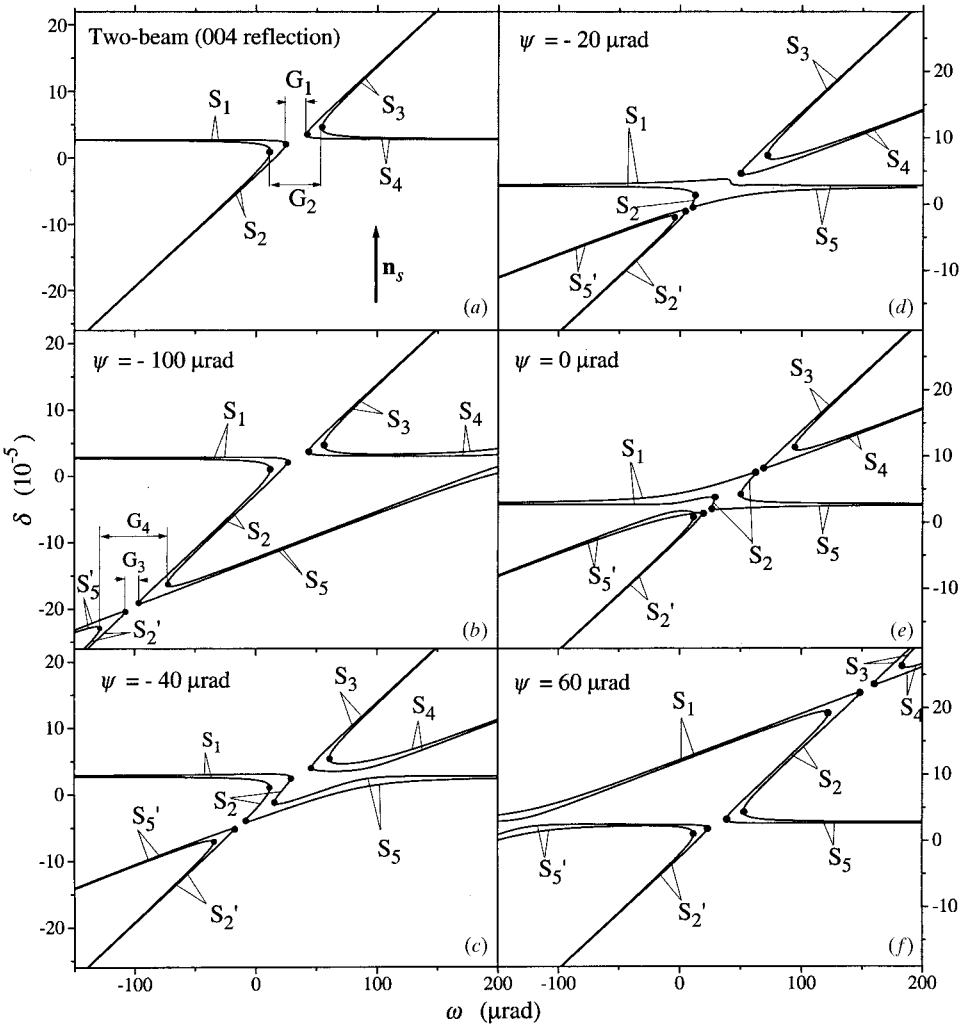

Figure 3
Sections of the DS for the GaAs 004|040 Bragg–Laue case. (*a*) Two-beam DS, 004 symmetric Bragg reflection. (*b*)–(*f*) Three-beam DS sections at different ψ angles. Each black dot represents the degenerate-root point (line) of a DS sheet. This unique point is used to unambiguously divide each sheet into two half sheets. Note that the three-beam full excitation center is near $\psi = -20$ μrad while $\psi = 0$ μrad corresponds to the geometrical diffraction center.

intensity profiles in Fig. 5 correspond to three representative phases $\pi/2$, π and $3\pi/2$, respectively. It is apparent that the principal features of all four profiles are very consistent with the general three-beam diffraction phenomena (Weckert & Hümmer, 1990; Hümmer *et al.*, 1990).

However, it is worth mentioning the *Aufhellung* effect in Fig. 5. This effect has been well known to be the intensity attenuation of the primary reflection **h** as a consequence of the energy transfer from **h** to the secondary reflection **g** *via* reflection $\mathbf{g}-\mathbf{h}$ (in contrast to the *Umweganregung* effect of intensity enhancement) (Mayer, 1928; Renninger, 1937). The *Aufhellung* effect is usually observed when reflection **h** is much stronger than **g** and is independent of the phase effect. But for the present semi-infinite-crystal case, where the reflections involved are all strong reflections with comparable strengths, the *Aufhellung* effect is still very strong.

4. Bragg–Bragg case

As a general principle for N-beam diffraction without grazing beams, there are always $2(N-N_B)$ boundary-condition equations (*i.e.* the continuity conditions of tangential displacement components) at the entrance surface, where N_B is the number of Bragg-reflected beams. For the semi-infinite-crystal case, since the back-surface boundary conditions do not exist, only $2(N-N_B)$ internal wave modes are allowed such that they can be constrained by the entrance-boundary conditions. This indicates that the Bragg–Bragg geometry of three-beam diffraction for a semi-infinite crystal is a two-mode process.

To demonstrate this, let us use the reflection pair $\mathbf{h}=004$ and $\mathbf{g}=1\bar{1}3$ in GaAs to construct the Bragg–Bragg geometry. When 004 is a symmetric Bragg reflection and $\lambda = 1.54$ Å, $1\bar{1}3$ is also a Bragg reflection. For this wavelength, the magnitudes of the structure factors involved are $|F_{000}| = 256$, $|F_{004}| = 163$, $|F_{1\bar{1}3}| = 126$, and $|F_{\bar{1}11}| = 155$. The related triplet phase Φ is very small and we artificially let it be zero for simplicity.

The evolution of the $004|1\bar{1}3$ DS with ψ is illustrated by the three sections in Fig. 6. It is obvious that the DS configuration of the Bragg–Bragg case is much different from that of the Bragg–Laue case. This difference results from the opposite signs of γ_g: $\gamma_g > 0$ for the Bragg–Laue case while $\gamma_g < 0$ for the Bragg–Bragg case. It is interesting that the DS sections in Fig. 6 are generally similar to the DS sections perpendicular to the reciprocal vector **h** (Hümmer & Weckert, 1996).

In Fig. 6(*a*), the three-beam DS can be considered to consist of two sets of two-beam Bragg reflection DS's: the left set is related to $1\bar{1}3$ and the right set corresponds to the primary reflection 004. The connection between these two sets of DS's is that they share two common segments labeled by S_1, and thus two *S*-shaped sheets are formed in the middle of Fig. 6(*a*) (Hümmer & Weckert, 1996). In Fig. 6(*b*) as the ψ angle is adjusted to be near the full three-beam diffraction center, the DS gaps are close to each other, giving rise to strong interaction between the two reflections. This is indicated by the significant distortion of segments S_1. When ψ becomes positively large, the DS gaps related to $1\bar{1}3$ move to the right (Fig. 6*c*) and the shape of the 004 DS again transforms asymptotically into that of the two-beam DS.

Based on the excitation mode of two-beam Bragg reflection discussed in §3, one can see immediately that, for the semi-infinite Bragg–Bragg case, tiepoints on the DS sheets labeled S_2, S_3, S_6 and S_7 in Fig. 6 are forbidden tiepoints. This indicates that for any incidence (ω, ψ) there are at most two tiepoints that are excited. If the incidence direction falls into the angular ranges where only one tiepoint is excited, the dispersion equation (5) has a pair of conjugate complex roots, of which only the one with a positive imaginary part is physically valid. Similarly, the angular ranges in which no tiepoint is excited correspond to the situation that (5) has two pairs of conjugate roots, of which only two roots are valid.

Therefore, the semi-infinite Bragg–Bragg case is indeed a two-mode diffraction process. The complex strengths q_j of the

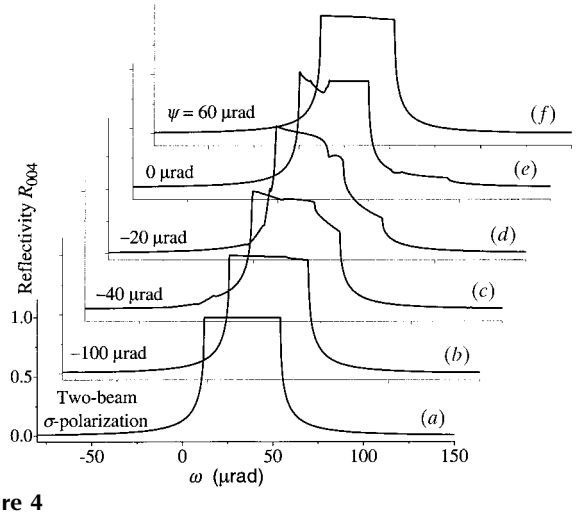

Figure 4
ω-scan rocking curves of 004 reflection in GaAs 004|040 three-beam diffraction. (*a*) Two-beam diffraction rocking curve. (*b*)–(*f*) Three-beam rocking curves corresponding to the DS sections in Figs. 3(*b*)–3(*f*), respectively.

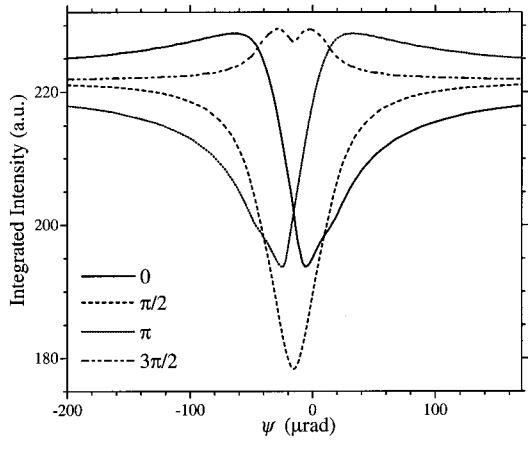

Figure 5
Integrated intensity profiles of the GaAs 004|040 three-beam diffraction calculated with artificially assigned invariant triplet phases $\Phi = 0, \pi/2, \pi$ and $3\pi/2$.

two eigenvectors can be determined by the two boundary equations at the entrance surface:

$$\sum_{j=1}^{2} q_j D_{0\sigma}^{(j)} = D_{\sigma}^{(a)}, \quad \sum_{j=1}^{2} q_j D_{0\pi}^{(j)} = D_{\pi}^{(a)}. \tag{10}$$

Subsequently, the amplitudes of the reflected beams are

$$\mathbf{D}_j^{(a)} = \boldsymbol{\sigma}_j \sum_{i=1}^{2} q_i D_{j\sigma}^{(i)} + \boldsymbol{\pi}_j \sum_{i=1}^{2} q_i D_{j\pi}^{(i)}, \tag{11}$$

where $j = h, g$.

The solid curves in Fig. 7(a) represent three 004 reflection ω-scan rocking curves calculated with (10) and (11), from which the transitions between the two- and three-beam cases can be seen clearly. The dashed lines are the ω-scan intensity profiles of the $1\bar{1}3$ reflection. Note that, for the $1\bar{1}3$ reflection, the ω-scan direction is a skew scan direction, which causes the difference between the two kinds of intensity profile.

Similar to the Bragg–Laue case, the correctness of the two-mode treatment can be seen from the fact that the reflectivity values of the two reflections, R_{004} and $R_{1\bar{1}3}$, are always less than or equal to 1. Such a principle remains valid even for the 'total reflectivity' $R_{004} + R_{1\bar{1}3}$. The total reflectivity profiles are plotted in Fig. 7(b). These profiles not only indicate clearly the energy conservation principle but also the total-reflection phenomenon in three-beam Bragg–Bragg diffraction.

5. Comparison with the thin-crystal case

For semi-infinite-crystal diffraction, there are always some specific wave modes that are forbidden according to the X-ray energy propagation inside the crystal, and the above examples have indicated that three-beam diffraction can be viewed as four- and two-mode diffraction processes for the Bragg–Laue and Bragg–Bragg geometries, respectively. In the thin-crystal case, all the wave modes can be excited due to the scattering from the back surface. Therefore, three-beam diffraction is a full six-mode process in thin crystals.

A typical example of thin-crystal diffraction is the parallel-plate model. For the Bragg–Bragg geometry, the strengths q_j of the six eigenvectors may be determined by boundary conditions at both the entrance and back surfaces. The entrance boundary conditions are the same as (10) and (11) except that here we have six wavefields. The back-surface boundary-condition equations have the form

$$\sum_{j=1}^{6} q_j D_{mn}^{(j)} \exp(2\pi i t K \delta_j) = 0, \tag{12}$$

where the δ_j's are the (complex) roots of (5), t is the crystal thickness, $m = h, g$ and $n = \sigma, \pi$. Figs. 8(a) and 8(b) show the ω-scan rocking curves of reflection 004 calculated with the six-mode computation procedure for two different plate-thickness values $t = 10$ and 50 µm, respectively. The dashed-line profile in Fig. 8(a) is the result calculated with the two-mode procedure for a semi-infinite crystal. As a typical phenomenon of thin-crystal diffraction (Batterman & Hildebrandt, 1968), the

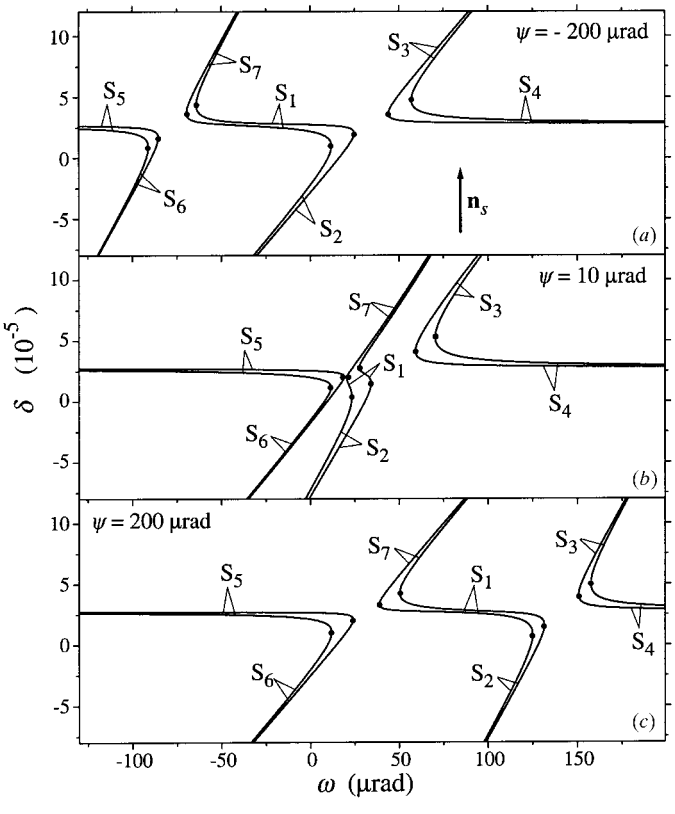

Figure 6
Typical DS sections of the GaAs 004/1$\bar{1}$3 three-beam diffraction, Bragg–Bragg geometry.

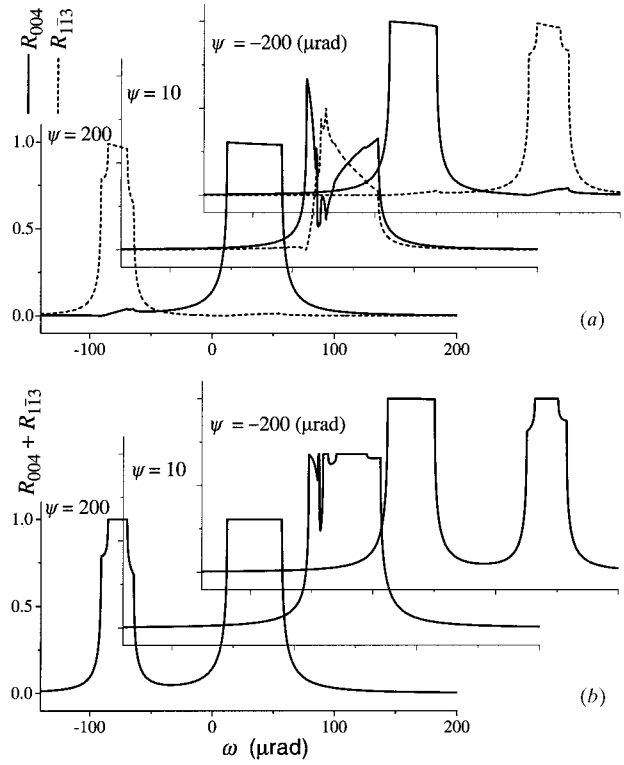

Figure 7
(a) ω-scan rocking curves of 004 and 1$\bar{1}$3 reflections calculated for a semi-infinite crystal. (b) Total reflectivity profiles.

six-mode intensity profiles are significantly modulated in the angular ranges besides the main peaks, and the oscillation frequency increases drastically with the crystal thickness. The irregular oscillation amplitudes in Fig. 8(*b*) indicate that the step used to calculate this profile was still too large compared to the extremely small oscillation period.

Compared to the nearly one-dimensional intensity oscillation in the two-beam case, the intensity modulation of the three-beam case is two-dimensional. This can be seen from the inset of Fig. 8(*a*), which shows the intensity oscillation along the ψ direction (for a fixed ω angle).

Apart from the intensity oscillation, the rocking curves calculated with the six-mode procedure are, in fact, very similar to that from the two-mode procedure. In particular, the intensities calculated by the two different procedures are extremely close to each other in the main peak ranges (extinction ranges). Authier (1996) has shown a similar phenomenon for the two-beam case even when absorption is considered. Here the similarity between the two kinds of rocking curve in Fig. 6 justifies again that the application of the two-beam tiepoint excitation rule to the three-beam case is successful for semi-infinite-crystal diffraction.

By artificially assigning four representative triplet phases to the GaAs 004|1$\bar{1}$3 reflections, we have calculated the corresponding ψ-scan integrated intensity profiles by two- and six-mode procedures, respectively. The results are shown in Fig. 9.

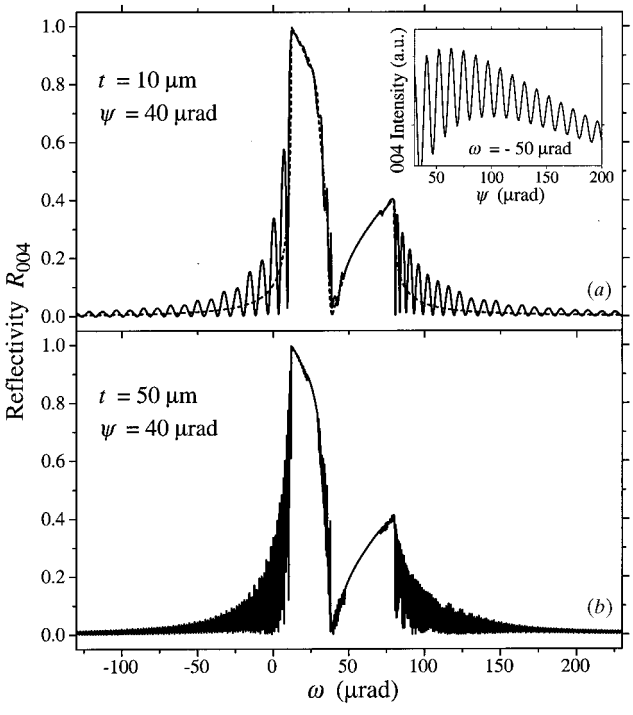

Figure 8
Intensity modulation calculated with the six-mode procedure. 004/1$\bar{1}$3 Bragg–Bragg diffraction in GaAs. (*a*) 004 ω-scan rocking curve at $\psi = 40$ μrad. Dashed line calculated with the two-mode procedure. Inset demonstrates the intensity oscillation along the ψ direction (intensity not integrated). (*b*) Short-period intensity oscillation in relatively thick plate.

Obviously, slight intensity oscillation can still be observed on the thin-crystal integrated intensity profiles. The other difference is that the thin-crystal diffraction intensities are stronger than those from a semi-infinite crystal although we have used the same parameters (except the thickness) to calculated these two sets of intensity profiles. The origin of this kind of difference needs further investigation. Nevertheless, the general features of the two kinds of profile are nearly the same.

6. Discussion and conclusions

Since we have totally ignored X-ray absorption in the above calculations, the results presented in this paper are mainly of theoretical interest. In reality, absorption may be regarded as a small perturbation to non-absorbing diffraction (Pinsker, 1978) but, in general, the influence of such a perturbation on thick-crystal diffraction intensities cannot be neglected. Owing to the limitation of our current root-searching method, we are not able to provide a real absorption example. However, from the two-beam diffraction picture, absorption has little impact on the DS configuration and on the basic diffraction principles. In this sense, the general diffraction mechanisms of three-beam diffraction from absorbing crystals are believed to be the same as that of the non-absorbing case.

To fully treat X-ray absorption in *N*-beam diffraction, one has to use the standard methods mentioned earlier to diagonalize the non-Hermitian scattering matrix so as to obtain the eigenvalues and eigenvectors. The eigenvalues (δ's) are generally complex even outside the extinction ranges for absorbing crystals. It has been pointed out that there are

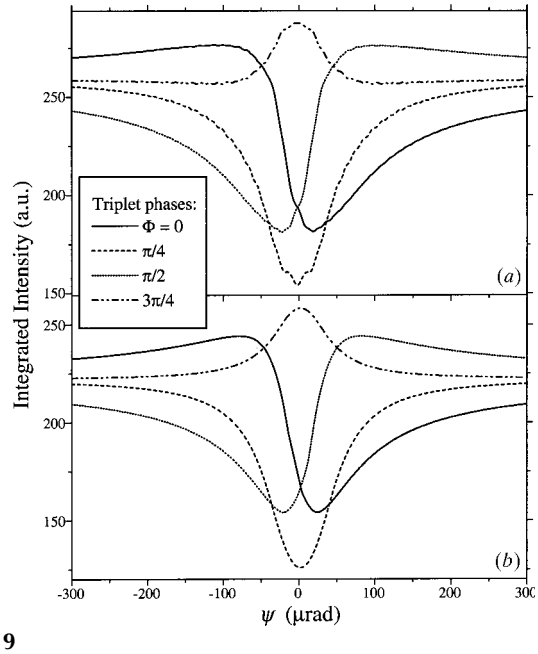

Figure 9
Integrated intensity profiles of the 004 reflection calculated for four representative invariant triplet phases, GaAs 004/1$\bar{1}$3 Bragg–Bragg case. (*a*) Thin crystal, thickness $t = 10$ μm. (*b*) Semi-infinite crystal.

always $2(N - N_B)$ wave modes that have damping amplitudes toward the inside of the crystals for Bragg-case N-beam diffraction (Pinsker, 1978; Hümmer & Billy, 1982; Stepanov & Ulyanenkov, 1994), and this principle has actually been proved by Chang (1979). Based on this principle, one can instead determine the excitation state of each wave mode from the sign of the imaginary part of the eigenvalue δ over the entire angular range of thick-crystal diffraction. This is of course a much simpler method for the semi-infinite-crystal approximation. From our illustrations above, one can see indirectly the origin of this principle.

In summary, through detailed analyses of the DS configurations in reciprocal space, we have demonstrated that there always exist forbidden wavefields in three-beam Bragg reflections from thick crystals. The excitation state of each wavefield inside the crystal can be strictly determined using the two-beam diffraction principle. Thus, three-beam diffraction in thick crystals is either a four-mode diffraction process for the Bragg–Laue geometry or a two-mode process for the Bragg–Bragg geometry. In each case, it was proved that the diffracted intensities can be completely determined by the entrance boundary conditions. Our calculations of non-absorbing crystal diffraction also revealed some other intrinsic properties of three-beam diffraction, including the extinction (total reflection) properties, the asymptotic transition between two- and three-beam diffraction, and the difference between thin- and thick-crystal diffraction. These illustrations could be helpful for one to understand the three-beam dynamical diffraction mechanisms.

The authors would like to thank Q. Shen for helpful discussions. The invaluable advice of the referees is also gratefully acknowledged. This work was partly supported by Cree Research, Inc. and the US Army Research Office under contract no. DAAG55-9810392.

References

Authier, A. (1996). *X-ray and Neutron Dynamical Diffraction: Theory and Applications*, edited by A. Authier, S. Lagomarsino & B. K. Tanner, pp. 1–31. New York: Plenum Press.
Batterman, B. W. & Hildebrandt, G. (1968). *Acta Cryst.* A**24**, 150–157.
Chang, S. L. (1979). *Acta Cryst.* A**35**, 543–547.
Chang, S. L. (1984). *Multiple Diffraction of X-rays in Crystals*. Berlin: Springer Verlag.
Chapman, L. D., Yoder, D. R. & Colella, R. (1981). *Phys. Rev. Lett.* **46**, 1578–1581.
Colella, R. (1974). *Acta Cryst.* A**30**, 413–423.
Høier, R. & Marthinsen, K. (1983). *Acta Cryst.* A**39**, 854–860.
Hümmer, K. & Billy, H. W. (1982). *Acta Cryst.* A**38**, 841–848.
Hümmer, K. & Billy, H. (1986). *Acta Cryst.* A**42**, 127–133.
Hümmer, K. & Weckert, E. (1996). *X-ray and Neutron Dynamical Diffraction: Theory and Applications*, edited by A. Authier, S. Lagomarsino & B. K. Tanner, pp. 345–367. New York: Plenum Press.
Hümmer, K., Weckert, E. & Bondza, H. (1990). *Acta Cryst.* A**46**, 393–402.
Juretschke, H. J. (1982). *Phys. Rev. Lett.* **48**, 1487–1489.
Mayer, G. (1928). *Z. Kristallogr.* **66**, 585–636.
Pinsker, Z. G. (1978). *Dynamical Scattering of X-rays in Crystals.* Berlin: Springer Verlag.
Press, H. W., Flannery, B. P., Teukolsky, S. A. & Vetterling, W. T. (1988). *Numerical Recipes in C*, 2nd ed., pp. 376–378. Cambridge University Press.
Renninger, M. (1937). *Z. Phys.* **106**, 141–176.
Shen, Q. (1986). *Acta Cryst.* A**42**, 525–533.
Shen, Q. (1998). *Phys. Rev. Lett.* **15**, 3268–3271.
Shen, Q. (1999). *Phys. Rev. Lett.* **83**, 4784–4787.
Shen, Q. (2000). *Phys. Rev. B*, **61**, 8593–8597.
Shen, Q. & Finkelstein, K. D. (1992). *Phys. Rev. B*, **45**, 5075–5078.
Stepanov, S. A. & Ulyanenkov, A. P. (1994). *Acta Cryst.* A**50**, 579–585.
Weckert, E. & Hümmer, K. (1990). *Acta Cryst.* A**46**, 387–393.
Weckert, E. & Hümmer, K. (1997). *Acta Cryst.* A**53**, 108–143.
Weckert, E. & Hümmer, K. (1998). *Cryst. Res. Technol.* **33**, 653–678.